International Journal of Heat and Fluid Flow 30 (2009) 319–330

Contents lists available at ScienceDirect

International Journal of Heat and Fluid Flow

journal homepage: www.elsevier.com/locate/ijhff

An eddy viscosity model with elliptic relaxation approach

M.M. Rahman *, T. Siikonen

Helsinki University of Technology, Department of Mechanical Engineering, Laboratory of Applied Thermodynamics, Sähkömiehentie 4, FIN-02015 HUT, Finland

ARTICLE INFO

Article history:
Received 7 January 2008
Received in revised form 4 August 2008
Accepted 17 December 2008
Available online 23 February 2009

Keywords:
Near-wall correction
Turbulence anisotropy
Realizability
Elliptic relaxation
Flow separation and reattachment

ABSTRACT

An extended version of the isotropic k—ϵ model accompanied by an elliptic relaxation approach to account for the distinct effects of low-Reynolds number (LRN) and wall proximity is proposed. To demonstrate the internal consistency of the elliptic relaxation approach with the characteristic length scale, both the Kolmogorov and hybrid length scales are introduced. The model incorporates a secondary source term to amplify the level of dissipation in nonequilibrium flow regions, thus reducing the kinetic energy and length scale magnitudes to improve prediction of adverse pressure gradient flows, involving flow separation and reattachment. The eddy viscosity formulation maintains the positivity of normal Reynolds stresses and the Schwarz' inequality for turbulent shear stresses. The model coefficients/functions preserve the anisotropic characteristics of turbulence. The model is validated against a few well-documented flow cases, yielding predictions in good agreement with the direct numerical simulation (DNS) and experimental data. Comparisons indicate that the present model offers considerable improvement over the standard eddy viscosity formulation.

1. Introduction

A large number of scientific and engineering calculations adhering to turbulent flows are established on the k—ϵ model due to its simplicity and effectiveness (Avva et al., 1988). However, an important prerequisite adhering to the appropriateness of a turbulence model is to represent the near-wall behavior of turbulence quantities accompanied by a preferential damping of velocity fluctuations in the direction normal to the wall that reconciles the influence of wall proximity adequately. Consequently, the near-wall modeling of turbulence has received extensive attention with the bulk of the effort directed toward two-equation models (Abe et al., 1997). The modeling of near-wall turbulence usually entangles distance to wall as an explicit parameter (Patel et al., 1985). This renders the model often inappropriate to simulating complex flows involving multiple surfaces, the wall distance of which becomes cumbersome to define. A remedy to this flaw is to develop a model which implicates no explicit wall distance while integrating it toward the solid surface (Park and Sung, 1997). In principle, near-wall turbulence includes both viscous and blocking (i.e., nonlocal) effects while low Reynolds number turbulence consists of the viscous effect alone (So et al., 1997). Consequently, the modification proposed for low-Reynolds number (LRN) turbulence is not necessarily applicable to near-wall flows.

The elliptic relaxation method is an excellent alternative to avoid the use of distance to wall (Durbin, 1991). The wall blocking is governed by an elliptic partial differential equation (i.e., Helmholtz-type equation) and naturally, nonlocal near-wall effects are taken into account. In fact, the primary objective of introducing the damping effect to closure models is to represent the kinematic blocking by the wall. The wall distance used in damping functions can be computed from a modified Poisson equation-based algorithm (Tucker, 1998, 2000; Fares and Schröder, 2000) similar to the elliptic relaxation equation. The difference is that the wall distance equation is solved only once (for fixed geometries), whereas the elliptic relaxation equation is solution dependent. The wall distance from the surface is uniquely defined as being the shortest distance between the present point and all no-slip boundaries in a flow field. The distance does not have to be measured normal to a surface. Even near the corner, it can be evaluated by introducing the limit of a wall with a very small curvature. The usual rationale of using the wall distance in the model functions is that the presence of the wall becomes very explicit to the turbulence model, and accordingly, the near-wall damping phenomenon is prosecuted. However, the wall distance method has several undesirable aspects relative to the elliptic relaxation approach. First, it needs several arguments and weighting factors to identify the nearest surface and locate the nearest corner and gap orientation (Tucker, 1998, 2000). Nevertheless, the later References (Tucker, 2003; Tucker et al., 2005) demonstrate that weighting factors are not needed for general turbulence modeling. Second, it requires smoothing parameters to enhance the iterative convergence (Fares and Schröder, 2000). Third, for moving geometries such a method turns out to be complicated and computationally expensive. Finally, it invokes an ad hoc/empirical damping function in which

* Corresponding author. Tel.: +358 9 4513994; fax: +358 9 4513418.
E-mail address: Mizanur.Rahman@tkk.fi (M.M. Rahman).

0142-727X/$ - see front matter © 2009 Elsevier Inc. All rights reserved.
doi:10.1016/j.ijheatfluidflow.2008.12.012

Nomenclature

b_{ij}	Reynolds stress anisotropy
C_f	friction coefficient
C_μ	eddy viscosity coefficient
E_ϵ	near-wall correction
f_μ	viscous damping function
L	characteristic length scale
h	channel height
k	turbulent kinetic energy
P	production of turbulent kinetic energy
Re_T	turbulence Reynolds number
S	mean strain rate
t	time
T_t	realizable time scale
u_τ	friction velocity
W	mean vorticity
y^+	nondimensional normal distance from the wall

Greek symbols

ζ	strain-rate/vorticity parameter
δ	half width of the channel
δ_{ij}	Kronecker's delta
ϵ	turbulent dissipation
μ, μ_T	laminar and eddy viscosities
ν	molecular kinematic viscosity
ρ	density
Π_b	turbulent anisotropy
σ	turbulent prandtl number

Subscripts

T	turbulent condition
ref	reference condition

the evaluated wall distance is to be implemented. The eddy viscosity damping function is often non-linear and, causes numerical inaccuracy and stiffness. The elliptic relaxation scheme avoids the complexity and, in essence, it is a natural choice to model the wall blocking effect.

A literature survey reveals that a few studies have attempted to abandon the use of wall distance by the elliptic relaxation. Durbin et al. (1994) explore an eddy viscosity μ_T transport equation that employs an elliptic relaxation equation of μ_T to avoid the need of damping functions. Nonlocal wall effects are taken into account by solving the μ_T equation and the length scales are determined locally without reference to the wall distance. The capability of the model is checked for a number of flow cases. However, a limited range of applicability is observed due to the improper account for the near-wall proximity, nonequilibrium and other complex turbulent properties. In fact, it is a rather difficult task to incorporate all these complexities into the μ_T equation without solving the k–ϵ transport equations. Park and Sung (1997) construct an eddy viscosity damping function f_μ as a product of empirical and elliptic relaxation functions. The empirical function may induce f_μ to grow, particularly in near-wall regions, thereby predicting excessive μ_T. In addition, the Kolmogorov length scale in the elliptic relaxation equation contains a large constant that has some precedent in the near-wall region. The model can be sensitive to this value (Durbin, 1991) and may degrade the results in comparison with experiments.

In a k–ϵ model approach, the k equation is relatively exact and essentially, the obvious choice is to modify the ϵ equation for enhancing the predictive capability. However, the modeled dissipation rate equation together with the near-wall correction is not always sufficient to provide the appropriate length scale of turbulence. For instance, the isotropic LRN k–ϵ eddy viscosity model with a constant C_μ, which is frequently used in computational fluid dynamics, performs quite well for boundary layer flows but fails badly for flows with a high mean shear rate or a massive separation. The possible reasoning is that the eddy viscosity is overpredicted. Basically, an overprediction of the eddy viscosity in the shear flow makes the model dissipative and therefore, causes the separation bubble to shorten. In addition, it violates the realizability constraints: the positivity of the normal Reynolds stresses and Schwarz' inequality between turbulent velocity correlations (Lumley, 1978). In order to improve the ability of the existing k–ϵ eddy viscosity model in predicting complex turbulent flows, the above-mentioned deficiencies should be removed.

Abandoning the wall distance approach to patch near-wall regions, the present study concentrates on near-wall and LRN modifications for the isotropic k–ϵ model where the integration up to the wall is extremely important. The improvement herein springs principally from the modeling of the elliptic relaxation function f_μ to suppress the excessive eddy viscosity in near-wall regions. The characteristic length scales (L_1 and L_2) associated with the elliptic relaxation equation are designed in terms of Kolmogorov and dynamic length scales in conjunction with the invariants of strain rate and vorticity tensors. Consequently, the large constant-dependent sensitivity of the relaxation function is reduced massively and the nonlocal effects are explicitly influenced by the mean flow and turbulent variables. The model incorporates an extra source term in the ϵ transport equation that augments the dissipation level in nonequilibrium flow regions, thus reducing the turbulent kinetic energy and length scale magnitudes to improve prediction of adverse pressure gradient flows involving separation and reattachment. The wall singularity is removed by using a physically appropriate time scale that never falls below the Kolmogorov (dissipative eddy) time scale, representing time scale realizability enforcement accompanied by the near-wall turbulent phenomena. The turbulent Prandtl numbers $\sigma_{(k,\epsilon)}$ are adjusted such as to provide substantial turbulent diffusion in the near-wall region. Furthermore, a modified coefficient C_μ that depends nonlinearly on both the rotational and irrotational strains is proposed based on the realizability constraints and appropriate experiments. Consequently, the model extends the ability of the two-equation model to account for nonequilibrium and anisotropic effects. Ostensibly, the new model is tensorially invariant, frame-indifferent and applicable to arbitrary topologies.

The performance of the new model is demonstrated through the comparison with experimental and DNS data of well-documented flows, consisting of a fully developed channel flow, turbulent free shear flows, a flat plate boundary layer flow with zero pressure gradient, a backward facing step flow and an asymmetric plane diffuser flow, respectively. The test cases are selected such as to justify the ability of the model to replicate the combined effects of LRN, near-wall turbulence and nonequilibrium.

2. Turbulence modeling

In collaboration with the Reynolds-averaged Navier-Stokes (RANS) equations, the proposed model determines the turbulence kinetic energy k and its dissipation rate ϵ by the following transport relations:

$$\frac{\partial \rho k}{\partial t} + \frac{\partial \rho u_j k}{\partial x_j} = \frac{\partial}{\partial x_j}\left[\left(\mu + \frac{\mu_T}{\sigma_k}\right)\frac{\partial k}{\partial x_j}\right] + \rho P - \rho \epsilon \tag{1}$$

$$\frac{\partial \rho\epsilon}{\partial t}+\frac{\partial \rho u_j\epsilon}{\partial x_j}=\frac{\partial}{\partial x_j}\left[\left(\mu+\frac{\mu_T}{\sigma_\epsilon}\right)\frac{\partial \epsilon}{\partial x_j}\right]+(C_{\epsilon 1}\rho P-C_{\epsilon 2}\rho\epsilon+E_\epsilon)/T_t \quad (2)$$

where ρ is the density, μ implies the molecular viscosity, $\sigma_{(k,\epsilon)}$ are the appropriate turbulent Prandtl numbers and the production term $P=-\overline{u_iu_j}(\partial u_i/\partial x_j)$. The Reynolds stresses $\rho\overline{u_iu_j}$ are related to the mean strain rate tensor S_{ij} through the Boussinesq approximation:

$$-\rho\overline{u_iu_j}=2\mu_T\left(S_{ij}-\frac{1}{3}S_{kk}\delta_{ij}\right)-\frac{2}{3}\rho k\delta_{ij},\quad S_{ij}=\frac{1}{2}\left(\frac{\partial u_i}{\partial x_j}+\frac{\partial u_j}{\partial x_i}\right) \quad (3)$$

Since the viscous dissipation presumably dominates near the wall, the turbulent viscosity is evaluated from

$$\mu_T=C_\mu f_\mu\rho kT_t \quad (4)$$

where the dynamic time scale k/ϵ is replaced by a realizable time scale T_t defined as

$$T_t=\sqrt{\frac{k^2}{\epsilon^2}+C_T^2\frac{v}{\epsilon}}=\frac{k}{\epsilon}\sqrt{1+\frac{C_T^2}{Re_T}},\quad Re_T=\frac{k^2}{v\epsilon} \quad (5)$$

where v denotes the kinematic viscosity and Re_T is the turbulence Reynolds number. Eq. (5) warrants that the eddy time scale never falls below the Kolmogorov time scale $C_T\sqrt{v/\epsilon}$, dominant in the immediate neighborhood of the solid wall. It prevents the singularity in the dissipation equation down to the wall. Alternatively, the turbulence time scale is k/ϵ at large Re_T but approaches the Kolmogorov limit $C_T\sqrt{v/\epsilon}$ for $Re_T\ll 1$. The empirical constant $C_T=\sqrt{2}$ associated with the Kolmogorov time scale is estimated from the behavior of k in the viscous sublayer (Rahman and Siikonen, 2001). Evidently, T_t in the ϵ equation guarantees near-wall asymptotic consistency without resorting to *ad hoc* damping functions employed in many k–ϵ models (Patel et al., 1985).

The extra source term E_ϵ in Eq. (2) is constructed from the most extensive turbulent diffusion models for k and ϵ equations derived by Yoshizawa (1987) with the two-scale direct-interaction approach using the inertial-range simplification. To receive positive benefits from the numerical reliability and to integrate the inertial-range condition directly to the solid wall, the cross-diffusion term is designed as (Rahman and Siikonen, 2000):

$$E_\epsilon=C_\epsilon\frac{\mu_T}{T_t}max\left[\frac{\partial(k/\epsilon)}{\partial x_i}\frac{\partial k}{\partial x_i},0\right],\quad C_\epsilon=\sqrt{C_{\epsilon 1}^2+C_{\epsilon 2}^2} \quad (6)$$

Obviously, $E_\epsilon>0$ in near-wall regions since $\partial(k/\epsilon)/\partial y>0$ and $\partial k/\partial y>0$. It can be argued that the source term E_ϵ stimulates the energy dissipation in nonequilibrium flows (Yoon and Chung, 1995), thereby reducing the departure of the turbulent length scale from its local equilibrium value and enabling improved prediction of adverse pressure gradient flows accompanied by flow separation and reattachment. At this stage, it appears necessary to identify that the quantity E_ϵ is characteristically beneficial in the vicinity of reattachment point and hence, it can be regarded as an attempt at replacing the Yap-correction (Yap, 1987).

The eddy viscosity damping function f_μ in Eq. (4) is obtained by solving the elliptic f_μ equation that envisages LRN and wall proximity effects. The model coefficient C_μ is in general a scalar function of the invariants formed on the strain rate S_{ij} and vorticity W_{ij} tensors in question (Pope, 1975; Gatski and Speziale, 1993). The vorticity tensor W_{ij} is defined as

$$W_{ij}=\frac{1}{2}\left(\frac{\partial u_i}{\partial x_j}-\frac{\partial u_j}{\partial x_i}\right) \quad (7)$$

The invariants of mean strain rate and vorticity tensors are defined by $S=\sqrt{2S_{ij}S_{ij}}$ and $W=\sqrt{2W_{ij}W_{ij}}$, respectively. The detailed functional form of C_μ is determined relying on the constraints such as realizability and appropriate experiments. The formulation of the model coefficients and associated relevant aspects are discussed in some detail in subsequent sections.

2.1. Coefficient C_μ and model realizability

The new model appears with recourse to the realizability constraints, reflecting physically necessary conditions for developing a compatible turbulence model. The realizability conditions are defined as (Lumley, 1978)

$$\overline{u_i^2}\geqslant 0,\quad \frac{\overline{u_iu_j}^2}{\overline{u_i^2}\,\overline{u_j^2}}\leqslant 1 \quad (8)$$

Eq. (8) also represents the minimal requirement to prevent a turbulence model from producing nonphysical results. The commonly used isotropic k–ϵ eddy viscosity model with a constant $C_\mu=0.09$ becomes unrealizable in the case of a large mean strain rate parameter T_tS (when $T_tS>3.7$), producing negative normal stresses and Eq. (8) is violated (Shih et al., 1995). To ensure realizability, the model coefficient C_μ cannot be a constant. It must be related with the mean flow deformation rate. Accordingly, a new formulation for C_μ as suggested by Gatski and Speziale (1993) is adopted:

$$C_\mu=\frac{\alpha_1}{1-\frac{2}{3}\eta^2+2\xi^2},\quad \eta=\alpha_2T_tS,\quad \xi=\alpha_3T_tW \quad (9)$$

The coefficients α_1–α_3 associated with Eq. (9) are given by

$$\alpha_1=g\left(\frac{1}{4}+\frac{2}{3}\Pi_b^{1/2}\right),\quad \alpha_2=\frac{3}{8\sqrt{2}g},\quad \alpha_3=\frac{2\sqrt{2}}{5}g,\quad g=\left(1+2\frac{P}{\epsilon}\right)^{-1} \quad (10)$$

where $\Pi_b=b_{ij}b_{ij}$ and the anisotropy of the Reynolds stress b_{ij} is defined as

$$b_{ij}=\frac{\overline{u_iu_j}}{2k}-\frac{1}{3}\delta_{ij} \quad (11)$$

Note that the constants associated with g are slightly modified to reproduce the data of DNS and experiments.

For homogeneous turbulent flows that are in equilibrium, Π_b and P/ϵ attain constant values, so that $\Pi_b\approx 0.11$ and $P/\epsilon=(C_{\epsilon 2}-1)/(C_{\epsilon 1}-1)\approx 1.9$. These values can be set in Eq. (10) to calculate inhomogeneous flows. However, the necessity to account for changes in Π_b and P/ϵ is appreciable since their equilibrium values drive the model to inconsistency in the context of a mild departure from equilibrium. For instance, Eq. (9) having constant coefficients is inadequate to guarantee a positive value of the coefficient and to provide nonnegative turbulent energy components. In addition, for sufficiently large strain rates η, singularities can occur. Girimaji (1996) has developed a fully-explicit, self-consistent variant of Gatski and Speziale (GS) by solving the cubic equation for P/ϵ. Nevertheless, the resulting solution for P/ϵ is unfortunately too cumbersome to be implement. Jongen and Gatski (1998) have extended the same GS model through a new approach to characterizing the equilibrium states of the Reynolds stress anisotropy in homogeneous turbulence. The model consists of a generalized relation for P/ϵ, integrating all planar homogeneous turbulent flows with/without rotation. To circumvent the problem in complex flows, compatible relations for Π_b and P/ϵ are devised with the assistance of Rahman and Siikonen (2003) that depend nonlinearly on both the rotational and irrotational strains:

$$\Pi_b=C_v\frac{P}{\epsilon},\quad \frac{P}{\epsilon}=C_v\zeta^2 \quad (12)$$

with

$$C_v=\frac{1}{2(1+T_tS\sqrt{1+R^2})},\quad \zeta=T_tS\max(1,R) \quad (13)$$

where $R = |W/S|$ is a dimensionless parameter that is very useful to characterize the flow. For instance, for a pure shear flow $R = 1$, whereas for a plane strain flow $R = 0$. It is appropriate to emphasize herein that introducing the auxiliary variables C_v and ζ, the proposed relation is constructed so as to meet the requirements of the equilibrium state: $P/\epsilon \approx 1$ with $\Pi_b \approx 0.09$ (that are very close to the DNS data: $P/\epsilon = 1$ and $\Pi_b \approx 0.095$) for the logarithmic region in a turbulent channel flow at $\zeta(R = 1) \approx 3.3$ (Kim et al., 1987) and $P/\epsilon \approx 1.9$ with $\Pi_b \approx 0.1$ for the homogeneous shear flow of Tavoularis and Corrsin (where $P/\epsilon \approx 1.9$ and $\Pi_b \approx 0.11$) at $\zeta(R = 1) \approx 6.0$ (Tavoularis and Corrsin, 1981), respectively.

Fig. 1 illustrates the distribution of P/ϵ as a function of shear parameter $\zeta(R = 1)$. As is evident, the relation Eq. (12) recovers the self-consistent models of Girimaji (1996) and Jongen and Gatski (1998) for the weak equilibrium condition. The new calibrated relations for Π_b and P/ϵ can assist the coefficients $(\alpha_1 - \alpha_3)$ in responding to both the shear and vorticity dominated flows that are far from equilibrium. The profile of C_μ is displayed in Fig. 2. Obviously, the C_μ distribution is in excellent agreement with various DNS data (Kim et al., 1987; Lee et al., 1990; Rogers and Moin, 1987) for pure shear flows (i.e., homogeneous shear flows with $R = 1$). The C_μ coefficient is reduced significantly with increasing ζ and maintained at a level that could mimic the complex turbulent flows. However, it seems likely that C_μ converges toward high values, i.e., $C_\mu = 0.25 - 0.3$ (here, in particular, compared with the traditional $C_\mu = 0.09$) as $0 < \zeta < 0.3$. In principle, the value of C_μ is very flow dependent and experimental evidences (Cazalbou and Bradshaw, 1993) indicate a range as large as $0.03 - 0.6$, substantiating the behavior of present C_μ worthily.

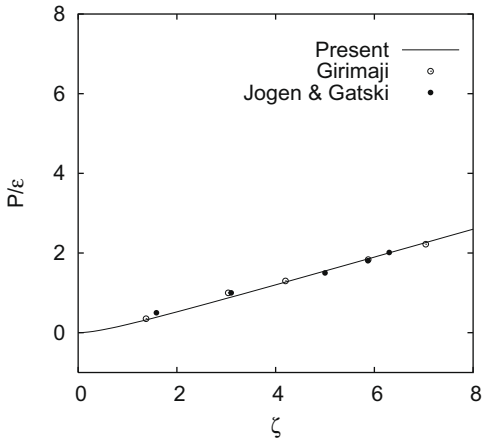

Fig. 1. Locus of solution points for state variable P/ϵ as a function of $\zeta(R = 1)$.

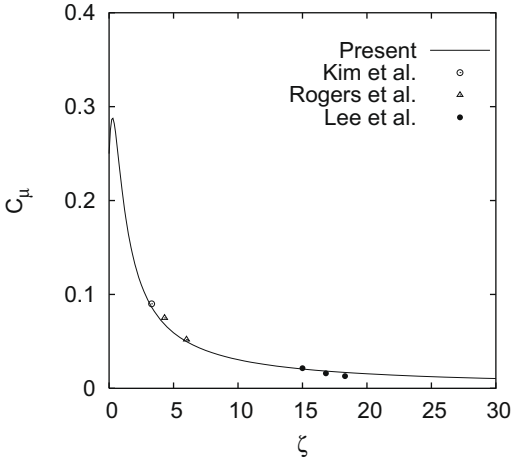

Fig. 2. Distribution of C_μ as a function of shear parameter ζ.

In particular, the following set of fundamental flows may play a pivotal role for the realizability analysis of the present model. The plane shear (i.e., homogeneous shear) flow, characterized by

$$S_{12} = S/2 = S_{21}, \quad W_{12} = S/2 = -W_{21} \tag{14}$$

is certainly an important example where the turbulence model needs to exhibit realizability. The flow field may either take the form of a boundary layer or a mixing layer (Rung et al., 1999). In this situation, it is not difficult to justify that the present formulation produces nonnegative energy components.

The model realizability is further contrasted with the accelerated flow where turbulence can be strongly attenuated (Rung et al., 1999). The turbulence attenuation is characterized by plane straining (where $R = 0$), traditionally called stretching, rather than shear. Herein, the most pronounced attenuation of turbulence kinetic energy is the evolution of the component $\overline{u_1 u_1}$ in the direction of a primary strain S_{11}. The fundamental stretching field together with the continuity equation for incompressible flow suggests that the limiting states are: the 2D stretching

$$S_{22} = -S_{11}(S_{33} = 0), \quad S_{11} = S/2 \tag{15}$$

and the axisymmetric stretching

$$S_{22} = S_{33} = -S_{11}/2, \quad S_{11} = S/\sqrt{3} \tag{16}$$

The two cases in question are often associated with irrotational plane strain and axisymmetric contraction of the flow, having different implications on the model realizability. In both cases, the realizability principle applied to the present model implies that

$$\frac{\overline{u_1 u_1}}{2k} = \frac{1}{3} - C_\mu T_t S_{11} \geqslant 0, \quad C_\mu = \frac{\alpha_1}{1 - \frac{2}{3}\eta^2} \tag{17}$$

The realizability principle pertaining to the 2–D plane strain and axisymmetric contraction states in Eq. (17) requires

$$\frac{3C_\mu\zeta}{2} \leqslant 1, \quad \sqrt{3}C_\mu\zeta \leqslant 1 \tag{18}$$

where $\zeta = T_t S$. With attention restricted to this flow situation, Eq. (12) can be recast as

$$\Pi_b^{1/2} = \frac{\zeta}{2(1+\zeta)}, \quad \frac{P}{\epsilon} = \frac{\zeta^2}{2(1+\zeta)} \tag{19}$$

It can be easily verified that with Eq. (19), the relation (18) is satisfied at a moderate strain rate. However, if $\zeta >> 1$, then $\zeta/(1+\zeta) \approx 1$. Therefore, $\Pi_b^{1/2} = 1/2$ and $P/\epsilon = \zeta/2$. In this case, the model coefficients assume the following values:

$$\alpha_1 = \frac{7}{12(1+\zeta)}, \quad \alpha_2 = \frac{3}{8\sqrt{2}(1+\zeta)}, \quad \eta = \frac{3\zeta}{8\sqrt{2}(1+\zeta)} = \frac{3}{8\sqrt{2}},$$
$$C_\mu \approx \alpha_1 = \frac{7}{12}(1+\zeta) \tag{20}$$

Consequently, with $C_\mu\zeta = 7/12$ one can certainly derive the conclusion that for $\zeta >> 1$, the inequality (18) is marginally satisfied for a 3D axisymmetric contraction of the flow. Above all, the present model does not exhibit unrealizable features at moderate (and compromisingly severe) strain rates.

Noteworthily, Eq. (17) provides the most critical situation in which C_μ faces the singularity problem or becomes negative. Nevertheless, these unexpected consequences are abandoned in favor of the modeled Π_b and P/ϵ as represented by Eqs. (12) and (19), (20).

2.2. Elliptic relaxation approach

The eddy viscosity damping function f_μ confronts the distinct effects of low-Reynolds number and wall proximity in near-wall regions, and can be devised pragmatically as

$$f_\mu = 1 - exp(-\lambda), \quad \lambda = \frac{y}{L} \tag{21}$$

where L is the characteristic length scale. To avoid the singularity close to the wall, the Kolmogorov length scale $(\nu^3/\epsilon)^{1/4}$ is generally added with the dynamic length scale $k^{3/2}/\epsilon$ (Durbin, 1991):

$$L^2 = \frac{k^3}{\epsilon^2} + C_\eta^2\sqrt{\frac{\nu^3}{\epsilon}} = \nu\left(Re_T\frac{k}{\epsilon} + C_\eta^2\sqrt{\frac{\nu}{\epsilon}}\right) \tag{22}$$

where C_η is a constant and evaluated empirically to replicate near-wall viscous effects. Alternatively, the second term in parenthesis is needed to obtain adequate wall blocking. Otherwise, the predicted turbulent viscosity will be too large near the wall. The length scale L is constructed such as to provide smoother switch between the Kolmogorov scale (small eddies) and the dynamic/integral scale (energy containing eddies).

In particular, detailed analysis of DNS data shows that the wall blocking effect is much stronger than the viscous/LRN effect (Manceau et al., 2001). The empirical approach to modeling the wall blocking effect is often inconsistent with the complex flows and may degrade the results considerably. To eradicate the complexity in defining the wall distance with multiple surfaces, a Helmholtz-type elliptic relaxation equation for f_μ is introduced. It represents a general ellipticity pertaining to f_μ without the knowledge of the wall distance. Ellipticity is desirable for a good convergence property (Armfield, 1991; Rahman et al., 1996). Differentiating Eq. (21) twice with respect to y yields an elliptic relaxation equation to account for the nonlocal nature of the wall effect:

$$\frac{\partial^2 f_\mu}{\partial y^2} = -(1-f_\mu)\left[\left(\frac{\partial\lambda}{\partial y}\right)^2 - \frac{\partial^2\lambda}{\partial y^2}\right] \tag{23}$$

A comparative assessment made of $\lambda_1^2 = (\partial\lambda/\partial y)^2$, $\lambda_2 = \partial^2\lambda/\partial y^2$ and $1/L^2$, constructed from DNS data (Mansour et al., 1988) at $Re_\tau = u_\tau\delta/\nu = 180$ is shown in Fig. 3. Herein, u_τ is the friction velocity and δ denotes the channel half-width. Comparisons are made by plotting the results in wall units. As is observed, λ_1^2 mimics the behavior of $1/L^2$ (i.e., $\lambda_1^2 \approx 1/L^2$) at a higher value of C_η associated with the Kolmogorov length scale in Eq. (22). However, λ_2 shows unexpected behavior in proximity to the wall and can be avoided for the following reasons: Fisrt, λ_2 has a minor contribution to Eq. (23) in the vicinity of the wall since $\lambda_2 << 1$. Second, to guarantee positivity and smoothness properties for the coefficient associated with the elliptic operator (i.e., $\partial^2/\partial y^2 = \nabla^2$). Finally, to gain some privilege over numerical computations. With this professed interest, Eq. (23) is justified to recast as

$$-L^2\nabla^2 f_\mu + f_\mu = 1 \tag{24}$$

The rationale with the present approach is that the wall proximity effect is modeled naturally in conjunction with the elliptic relaxation function f_μ and hence nonlocal effects such as wall blocking. The virtue of Eq. (24) is that unlike the Poisson equation, it requires no special numerical treatment (i.e., the Laplace operator is relatively easy to treat, but particularly easy is the modification $-L^2\nabla^2 + 1$). It can be solved in parallel with the k–ϵ equations having an initial guess $0 \leqslant f_\mu \leqslant 1$ everywhere except on wall boundaries where $f_\mu = 0$.

In principle, the length scale in Eq. (22) needs to be tuned consistently at the appropriate DNS/experimental data to evaluate the LRN/near-wall turbulence (Durbin, 1991). It seems likely that the Kolmogorov length scale plays an important role in modeling the near-wall turbulence (Fig. 3). To demonstrate the internal consistency of the elliptic relaxation approach with the Kolmogorov/hybrid length scale and its effect on different flow types, the following compatibility relations are deduced after some manipulations:

$$L_1^2 = \zeta(3\zeta + C_\mu Re_T)\sqrt{\frac{\nu^3}{\epsilon}}, \quad L_2^2 = \nu\left(\frac{C_\mu}{3}Re_T\frac{k}{\epsilon} + 3\zeta^2\sqrt{\frac{\nu}{\epsilon}}\right) \tag{25}$$

where L_1 denotes a pure Kolmogorov length scale and L_2 is the hybrid (Kolmogorov and dynamic) length scale. Both the length scales L_1 and L_2 contain some multiplying factors to fit the data, for instance, the DNS data for developed channel flows. Conspicuously, the strain rate/vorticity parameter associated with the Kolmogorov length scale in Eq. (25) reduces the large constant dependency of the relaxation function f_μ as mentioned by Durbin (1991). In other words, the anisotropic coefficients associated with the length scale indubitably are conducive to allowing compatible changes in Kolmogorov and dynamic length scales that account for the anisotropy of near-wall turbulence. Actually, the whole flow domain of the elliptic Helmholz Eq. (24) is influenced by the walls and the solution of (24) relaxes to 1 (one) far from the wall. Hence, the present proposal can be thought of as an interpolation method between near-wall and free turbulence, with the interpolation coefficient provided by a nonlocal model.

A plot of $C_\mu f_\mu$ against the DNS data (Mansour et al., 1988) for fully developed turbulent channel flows is shown in Fig. 4 and good correlation is obtained. In these figures, the abbreviations L1M and

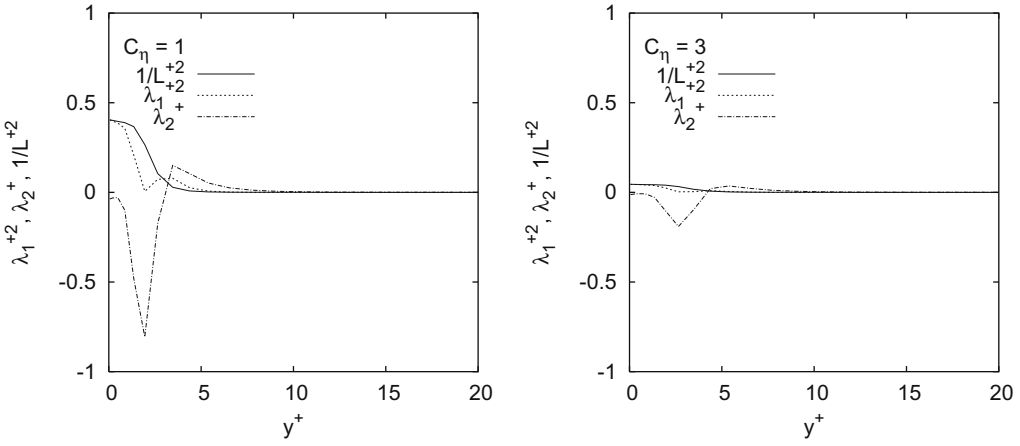

Fig. 3. Comparative assessment of scaling parameters at different values of C_η with $Re_\tau = 180$.

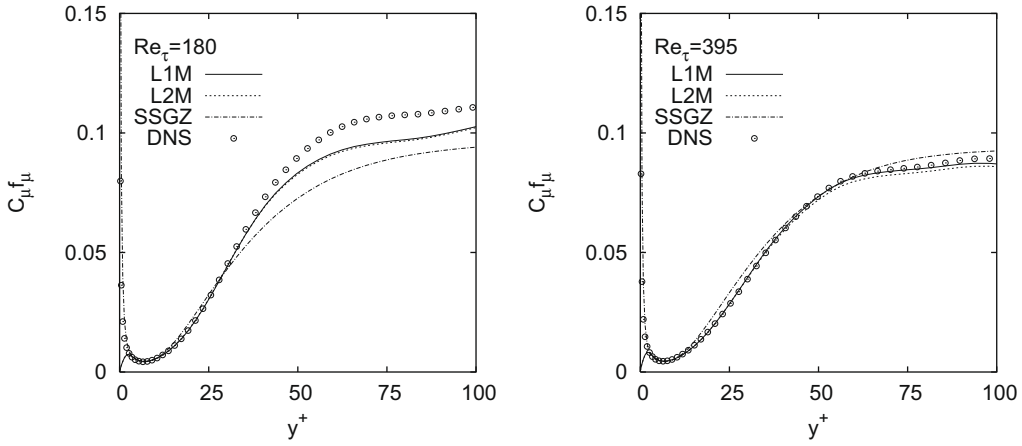

Fig. 4. Variations of eddy viscosity coefficient with wall distance in channel flows.

L2M stand for the present models with the length scales L_1 and L_2, respectively. Effectively, the results of Eq. (24) are given with the two length scales L_1 and L_2. The result of the SSGZ model (So et al., 1997) is also included for comparison. The elliptic function f_μ in Eq. (24) is valid in the whole flow field, including the viscous sublayer and the logarithmic layer. In the region close to the wall, the Reynolds stress $-\overline{uv} \sim y^3$ and $k \sim y^2$. To preserve the correct cubic power-law behavior of $-\overline{uv}$, the damping function (herein the product $C_\mu f_\mu$) needs to increase proportionally to y^{-1} in the near-wall region. As is evident by Fig. 4 in comparison with the DNS data, the adopted form of $C_\mu f_\mu$ reproduces the asymptotic limit involving the distinct effects of LRN and wall proximity. The product $C_\mu f_\mu \approx 0.09$ (the standard choice for $C_\mu = 0.09$, pertaining to the linear k–ϵ model) remote from the wall to ensure that the model is compatible with the standard k–ϵ turbulence model. The use of elliptic relaxation function f_μ confronts the singularity at neither the separating nor the reattaching point in contrast to the adoption of $y^+ = u_\tau y/\nu$. Consequently, the model is applicable to separated and reattaching flows.

2.3. Other model coefficients

Near-wall flows show a tendency to underestimate the dissipation rate ϵ due to the local anisotropy of turbulence, adhering to the non-dimensional parameter P/ϵ (Durbin and Speziale, 1991). Researchers allow the coefficient $C_{\epsilon 1}$ to be a function of P/ϵ with a view to enhancing dissipation in such a situation (Durbin, 1993; Ahn et al., 1997). However, in some of the more complex flows that have been calculated, the dependence on P/ϵ prevents numerical convergence to a steady state (Durbin, 1995). One possible approach to counteracting this adverse situation is to explore alternative elements with relevance to P/ϵ:

$$C_{\epsilon 1} = 1 + \frac{\Pi_b^*}{C_T}, \quad C_{\epsilon 2} = C_T \tag{26}$$

where $\sqrt{\Pi_b^*} = C_\mu \zeta$ is essentially identical to Eq. (12), however, with the exception that C_v is replaced by C_μ. It can be stressed that the rational subsistence Π_b^* to P/ϵ certainly induces compatible changes in $C_{\epsilon 1}$ which accounts for the additional production of dissipation by the anisotropy of turbulence. It has been shown in Section 2.1 that $\sqrt{\Pi_b^*} = C_\mu \zeta$ attains a maximum value of 7/12, indicating a range of $C_{\epsilon 1}$ = 1–1.24. Herein, one remarkable departure from the conventional modeling needs to be noted. The coefficient $C_{\epsilon 1}$ is made a function of the invariants, while $C_{\epsilon 2}$ is reduced from its usual value of 1.92 to $C_T = \sqrt{2}$. Nevertheless, $C_{\epsilon 2}/C_{\epsilon 1} \approx 1.33$ in the log layer of a channel flow with $\zeta(R = 1) \approx 3.3$, converging toward the standard $C_{\epsilon 2}$-to-$C_{\epsilon 1}$ ratio ($1.92/1.44 = 1.33$).

In particular, a relatively small $(C_{\epsilon 2} - C_{\epsilon 1})$ compared with the conventional (1.92–1.44) may lead to some discrepancies in the free-stream velocity/turbulence decay. In this case, the $C_{\epsilon(1,2)}$ values can be adjusted in order to reproduce the correct decay. However, the computations of the free jet and flat plate cases show that the modifications do not seriously affect the results. In fact, any nonlinear correction to μ_T (that results in a considerable reduction in μ_T compared with μ_T, having a constant C_μ) is dispersive rather than dissipative – a feature that slows down the convergence. The jointly reduced values of $C_{\epsilon(1,2)}$ may recover the convergence enhancement to some extent. In addition, the modifications assist qualitatively in predicting turbulent flows with separation and reattachment.

The budgets of k and ϵ from the *DNS* data suggest that the role of turbulent diffusion in the near-wall region is substantial. Accordingly, the Prandtl numbers σ_k and σ_ϵ are modeled, rather than being assigned constant values (unlike the commonly adopted practice with $\sigma_k = 1.0$, and $\sigma_\epsilon = 1.3$):

$$\sigma_k = \frac{4}{1 + 2\zeta} + f_\mu^2, \quad \sigma_\epsilon = \frac{4C_T}{1 + 2\zeta} + f_\mu^2 \tag{27}$$

The model coefficients σ_k and σ_ϵ are developed so that sufficient diffusion is obtained in the vicinity of the wall. This contrivance tends to successfully predict the kinetic energy and dissipation rate profiles (Abe et al., 1997). The issue of the σ_ϵ formulation deserves further attention: the connection between the von Karman constant κ and the difference $(C_{\epsilon 2} - C_{\epsilon 1})$. The log-region analysis shows that κ is given by $\kappa^2 = \sigma_\epsilon (C_{\epsilon 2} - C_{\epsilon 1}) \sqrt{C_\mu}$. For the logarithmic region in a turbulent channel flow at $\zeta(R = 1) \approx 3.3$ (Kim et al., 1987), $C_\mu \approx 0.09$, $f_\mu \approx 1$ and $C_{\epsilon 1} \approx 1.064$, and the von Karman constant thus determined is $\kappa \approx 0.42$. The developed channel flow results in the validation section show that the log law is recovered.

2.4. Boundary conditions

The transport equations for k and ϵ are subjected to the following boundary conditions at solid walls:

$$k_w = 0, \quad \epsilon_w = 2\nu \left(\frac{\partial \sqrt{k}}{\partial y} \right)^2 \approx 2\nu \frac{k}{y^2} \tag{28}$$

To avoid numerical instability, the approximation for ϵ_w is applied at the first grid node neighboring the wall, rather than on the wall itself. This requires normal distance from a wall to the nearest grid point, which is unambiguous and readily available. The validity of Eq. (28) necessitates that the grid system is fine enough to produce the near-wall limiting behavior.

3. Computations

To validate the generality and efficacy of the proposed model, a few applications to two-dimensional turbulent flows consisting of a fully developed channel flow, turbulent free shear flows, a flat plate boundary layer flow with zero pressure gradient, a backward facing step flow and an asymmetric plane diffuser flow are considered. To convince the readers toward the model reliability and accuracy, the present model predictions are compared with those from the SSGZ model (So et al., 1997). The SSGZ model contains a near-wall correction term with $C_\mu = 0.09$. Furthermore, it uses the Kolmogorov velocity scale in the eddy viscosity damping function to account for near-wall effects. Therefore, the SSGZ model is supposed to evaluate the combined effects of LRN and near-wall turbulence with reasonable accuracy, as reported by So et al. (1997). However, compared with the SSGZ model, the new model is additionally sensitized to nonequilibrium and anisotropic effects.

A cell centered finite-volume scheme combined with an artificial compressibility approach is employed to solve the flow equations (Rahman et al., 1997; Rahman and Siikonen, 2001). A fully upwinded second-order spatial differencing is applied to approximate the convective terms. Roe's (Roe, 1981) damping term is used to calculate the flux on the cell face. A diagonally dominant alternating direction implicit (DDADI) time integration method (Lombard et al., 1983) is applied for the iterative solution to the discretized equations. A multigrid method is utilized for the acceleration of convergence (Jameson and Yoon, 1986). The basic implementation of the artificial compressibility method and associated features are described elsewhere (Rahman et al., 1997; Rahman and Siikonen, 2001). Note that the elliptic relaxation Eq. (24) is solved using a tridiagonal matrix algorithm (TDMA). In every coordinate direction, the implicit stage performs typically two sweeps that provide convincingly the converged state for f_μ at each iteration level.

A variable grid spacing is used to resolve the sharp gradient in near-wall regions. Grid densities are varied to ensure the grid independence of the numerical results. It is found that the solution is not sensitive to the number of grid points as long as there are two points in $y^+ < 1.5$. In the computations that follow, convergence is judged by monitoring the root-mean-square residuals of flow variables. The solution is taken as having converged when all residuals are of the order of 10^{-4} or less. This means that no appreciable changes are found in the residuals.

3.1. Channel flow

The computation is carried out for a fully developed turbulent channel flow at $Re_\tau = 395$ for which turbulence quantities are attainable from the DNS data (Mansour et al., 1988). The calculation is conducted in the half-width of the channel, imposing periodic boundary conditions, except for the pressure, pertaining to the upstream and downstream boundaries. The computation involving a 64×48 nonuniform grid refinement is considered to be sufficiently accurate to describe the flow characteristics. For this case, the length of the computational domain is 32δ. To ensure the resolution of the viscous sublayer the first grid node near the wall is placed at $y^+ \approx 0.3$. Comparisons are made by plotting the results in the form of $u^+ = u/u_\tau$, $k^+ = k/u_\tau^2$, $\overline{uv}^+ = \overline{uv}/u_\tau^2$ and $\epsilon^+ = \nu\epsilon/u_\tau^4$ versus y^+.

Fig. 5 shows the velocity profiles for different models. The prediction of the L1M and L2M (present models) agree well with the DNS data. The SSGZ model slightly underestimates the mean velocity profile in the outer layer. Profiles of turbulent shear stresses are displayed in Fig. 6. Agreement of all model predictions with the DNS data seems to be satisfactory.

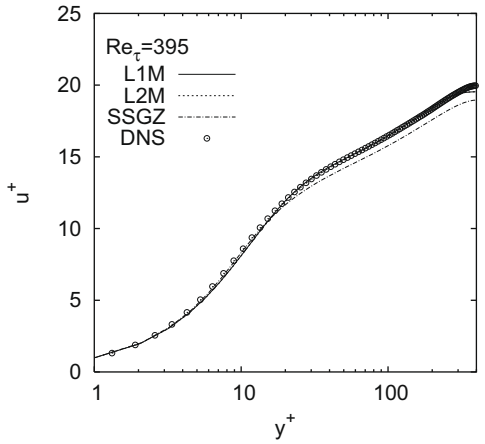

Fig. 5. Mean velocity profiles of channel flow.

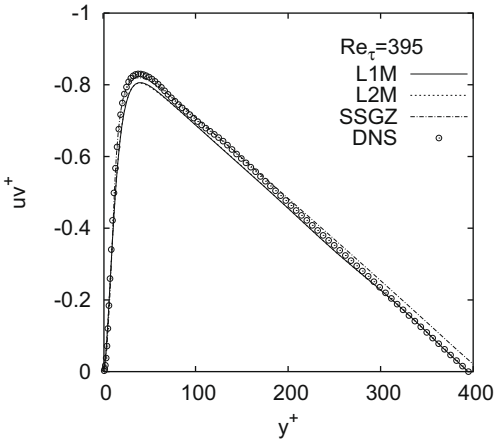

Fig. 6. Shear stress profiles of channel flow.

Further examination of the model performances is directed to the k^+ profiles as portrayed in Fig. 7 for the near-wall region. As is evident, the present model predictions are in broad accord with the SSGZ model and DNS data. Fig. 8 exhibits the profiles of ϵ^+ from the three computations. The present as well as the SSGZ model provides a maximum ϵ^+ at the wall which is more in line with the experimental and DNS data.

3.2. Turbulent free shear flows

The objective of this validation is to demonstrate that the modified turbulent Prandtl numbers $\sigma_{(k,\epsilon)}$ and the extra source term E_ϵ in Eq. (2) do not seriously affect the computations of free jets. Calculations are performed for a plane jet and a round jet. Figs. 9 and 10 show the comparisons of the self-similar mean velocity profiles from the model predictions and the various measurements for the plane and round jets respectively. The mean axial velocity u is normalized by the centerline velocity u_c. In Fig. 9 the model predictions are compared with the measurements of Bradbury (1965) and Heskestad (1965) for the plane jet. All three models agree well with the data. However, especially in the outer region the comparison with the experimental data evidences a slight superiority of the SSGZ model over the present models. This is probably because the new model invokes a relatively small $(C_{\epsilon 2} - C_{\epsilon 1})$ compared with the SSGZ model. The modified $\sigma_{(k,\epsilon)}$ and E_ϵ have minor effects on this behavior. Shown in Fig. 10 are the comparisons between the model predictions and the measurements of Rodi (1975), and

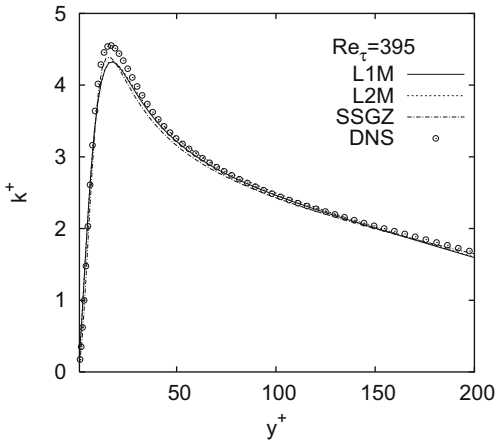

Fig. 7. Turbulence kinetic energy profiles of channel flow.

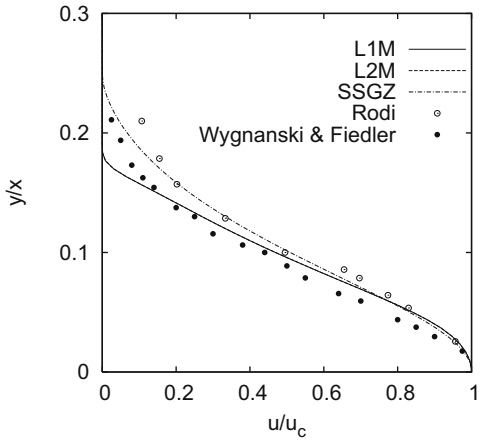

Fig. 10. Comparison of computed and measured velocity profiles for round jet.

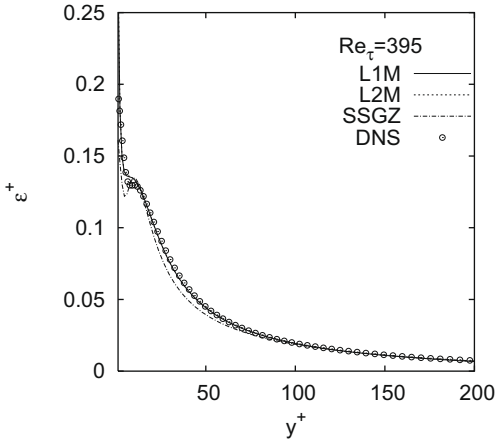

Fig. 8. Dissipation rate profiles of channel flow.

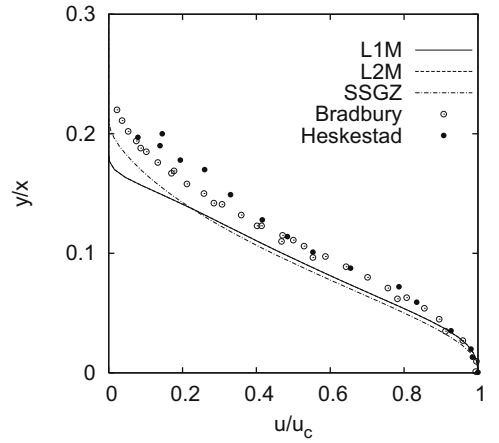

Fig. 9. Comparison of computed and measured velocity profiles for plane jet.

Wygnanski and Fiedler (1969) for the round jet. All three models give likewise accurate predictions of the flow with a smooth approach to the freestream velocity. No appreciable differences are observed in the predictions of the present L1M and L2M for both plane and round jet computations.

The spreading rate is generally defined as the value of y/x where the velocity is half its centerline (maximum) value. The spreading rates given in Table 1 provide a concise criterion of the predictive capabilities of the turbulence models for free shear layers and confirm the quality of the new model. Both the present and SSGZ models predict a slightly lower spreading than indicated by the experiment for the plane jet. Nevertheless, the predicted spreading rates of the present models fall within the range of measured values for the round jet. In this case, the SSGZ model slightly overpredicts the magnitude.

3.3. Flat plate boundary layer flow

The performance of the proposed model is further contrasted with the experimental data of the flow over a flat plate with a high free stream turbulence intensity. The test case is taken from ERCOFTAC Fluid Dynamics Database WWW Services (http://ercoftac.mech.surrey.ac.uk/) reported by John Coupland at Rolls-Royce. Measurements down to $x = 1.495$ m which corresponds to $Re_x \approx 94000$, are made by Roach and Brierly (1992). The inlet velocity is 9.4 m/s and the pressure gradient is zero. The upstream turbulence intensity $Tu = 6.0\%$, defined as $Tu = \sqrt{\frac{2}{3}k}/U_{ref}$, where U_{ref} indicates the reference (inlet) velocity. The dissipation is set so that the decay of free stream turbulence is in balance (Chen et al., 1998).

Computations begin 16 cm ahead of the leading edge where the symmetric conditions are applied. The length and height of the grid are 1.6 m and 0.3 m, respectively. The near-wall grid node is located at $y^+ < 1.0$, except the point at the leading edge ($y^+ = 2.1$). The grid size is 96×64 and heavily clustered near the wall.

The predicted skin friction coefficients ($C_f = 2u_\tau^2/U_{ref}^2$) are compared with the experimental data in Fig. 11. Savill's investigation (Savill, 1993) approves that the Launder and Sharma (LS) model is one of the best models for the prediction of transition points. Therefore, the LS model (Launder and Sharma, 1974) computation is plotted for comparison. The SSGZ model basically predicts transition too early. However, other models exhibit an interesting feature that the transition starts at the right position and it is strong enough. Both the LS and present models (L1M and L2M) return the skin friction in terms of its magnitude and trend with satisfac-

Table 1
Spreading rates for turbulent free shear flows.

Flow	SSGZ	L1M	L2M	Measured
Plane jet	0.091	0.097	0.097	0.10–0.11
Round jet	0.101	0.095	0.095	0.086–0.096

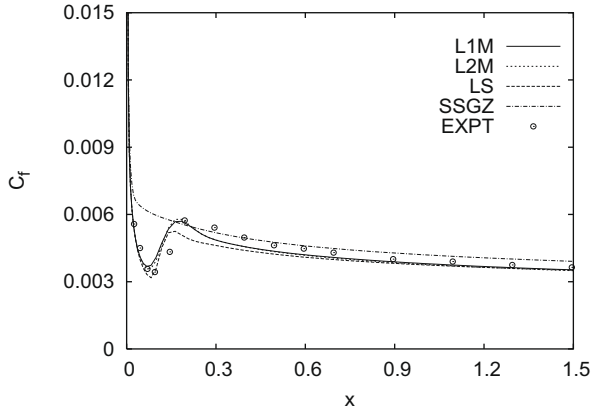

Fig. 11. Streamwise skin friction coefficient of boundary layer flow.

tory accuracy. No remarkable difference is observed in predictions adhering to L1M and L2M.

3.4. Backward facing step flow

To ascertain the performance in complex separated and reattaching turbulent flows, the present model is applied to the flow over a backward facing step. The computations are conducted corresponding to the experimental case with zero deflection of the wall opposite to the step, as investigated by Driver and Seegmiller (1985). The reference velocity $U_{ref} = 44.2$ m/s and the step height $h = 0.0127$ m. The ratio between the channel height and the step height is 9, and the step height Reynolds number is $Re = 3.75 \times 10^4$. At the channel inlet, the Reynolds number based on the momentum thickness is $Re_\theta = 5.0 \times 10^4$.

For the computations, grids are arranged in two blocks. The smaller one (extended from the inlet to the step) contains a 16×48 nonuniform grid and the grid size for other one is 120×80. The maximum height of the first near-wall grid node is at $y^+ < 1.5$. The inlet conditions are specified four step heights upstream of the step corner and the outlet boundary conditions are imposed 30 step heights downstream of the step corner. The inlet profiles for all dependent variables are generated by solving the models at the appropriate momentum thickness Reynolds number. The distance x/h is measured exactly from the step corner.

Computed and experimental friction coefficients C_f along the step side wall are plotted in Fig. 12. As is observed, all models are in good agreement with the data. However, the SSGZ model exhibits a nonphysical trend in the C_f profile near the corner at the base of the step. This is probably due to the improper behavior of the viscous damping functions employed. The positive C_f that starts from $x/h = 0$ is due to a secondary eddy which sits in the corner at the base of the step, inside the main recirculation region. The recirculation lengths predicted by the present (L1M and L2M) and SSGZ models are $6.4h$ and $6.0h$, respectively. The experimental value of the reattachment length is $(6.26 \pm 0.1)h$, making a fairly good correspondence with the models. A closer inspection of the C_f distribution indicates that L1M differs slightly from L2M in the recovery region.

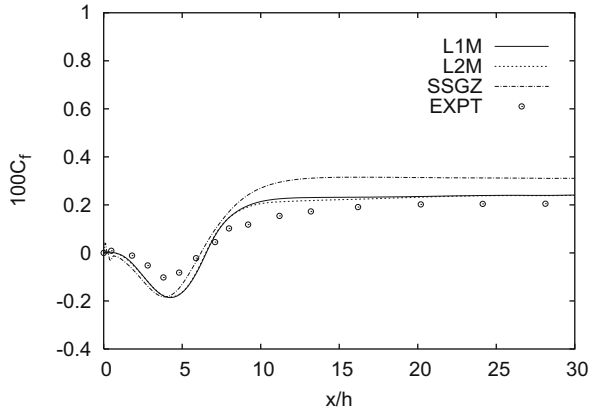

Fig. 12. Skin friction coefficient along the step-side bottom wall.

3.5. Asymmetric plane diffuser flow

To validate the performance in complex separated and reattaching turbulent flows, the present model is applied to the flow in an asymmetric diffuser with an opening angle of 10°, for which measurements are available (Buice and Eaton, 1997). The expansion ratio of 4.7 is sufficient to produce a separation bubble on the deflected wall. Hence the configuration provides a test case for smooth, adverse pressure driven separation. The entrance to the diffuser consists of a plane channel to invoke fully developed flow with $Re = 2.0 \times 10^4$ based on the centerline velocity U_{ref} and the inlet channel height h. Computations involving a 120×72 nonuniform grid resolution are considered to be accurate to describe the flow characteristics. The length of the computational domain is $76h$. The thickness of the first cell remains below one in y^+ units on both the deflected and flat walls.

Fig. 13 portrays the predicted skin friction coefficients C_f. The performance of the present model (L1M and L2M) evinces an encouraging qualitative agreement with measurements. As is ob-

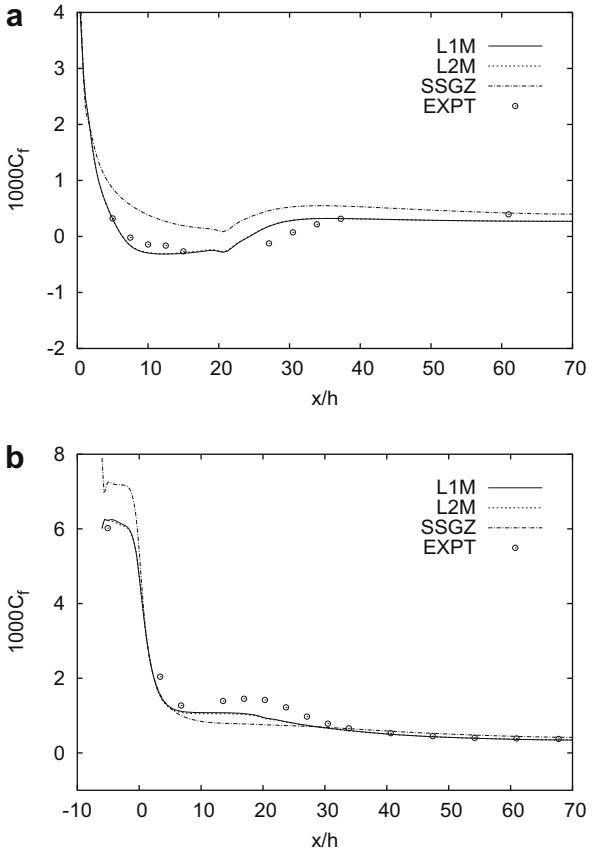

Fig. 13. Skin friction coefficients of diffuser flow: (a) along the deflected bottom wall and (b) along the straight top wall.

served, the SSGZ model predicts C_f distribution with an overshoot along the deflected bottom wall and gives no flow separation. Apparently, this ambiguous prediction regarding the SSGZ model demands a higher value for the proposed near-wall correction in the ϵ equation to render the model results compatible with the experiment.

Fig. 14 exhibits the mean velocity profiles at three representative positions. The performance of all models in predicting the

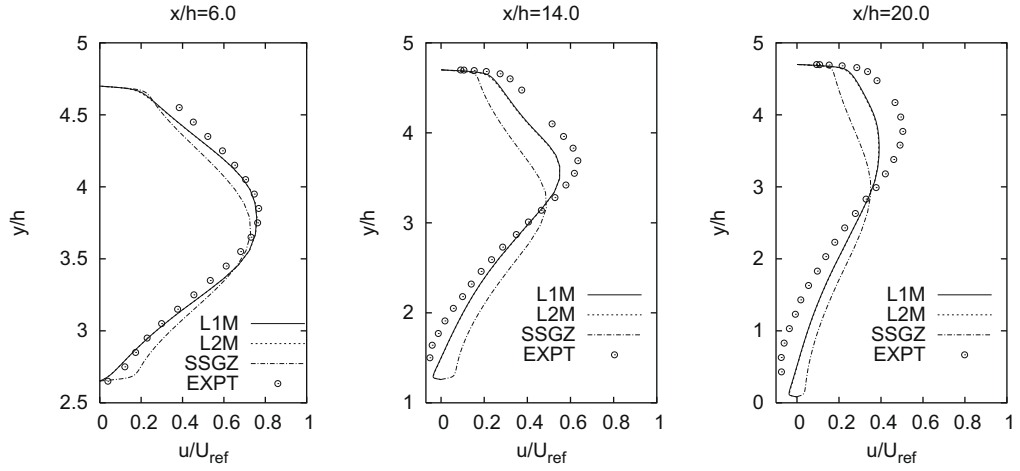

Fig. 14. Mean velocity profiles at selected locations for diffuser flow.

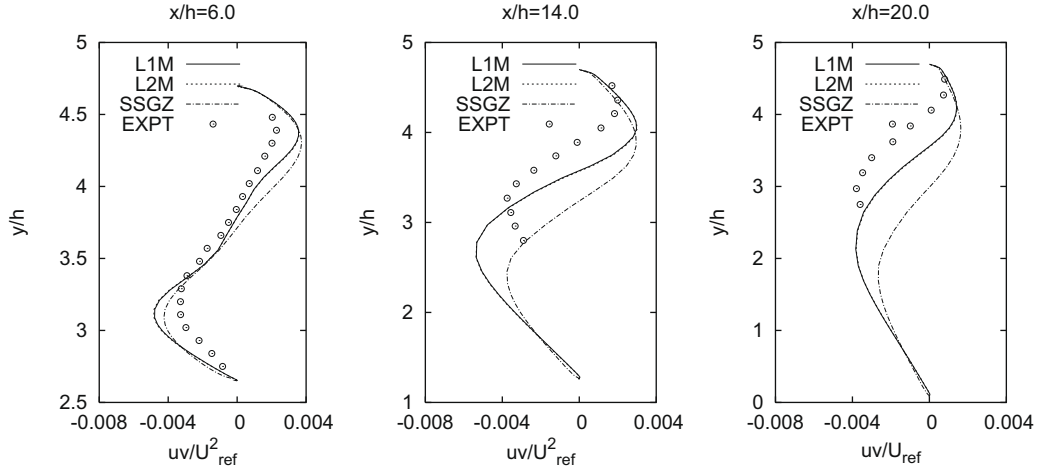

Fig. 15. Shear stress profiles at selected locations for diffuser flow.

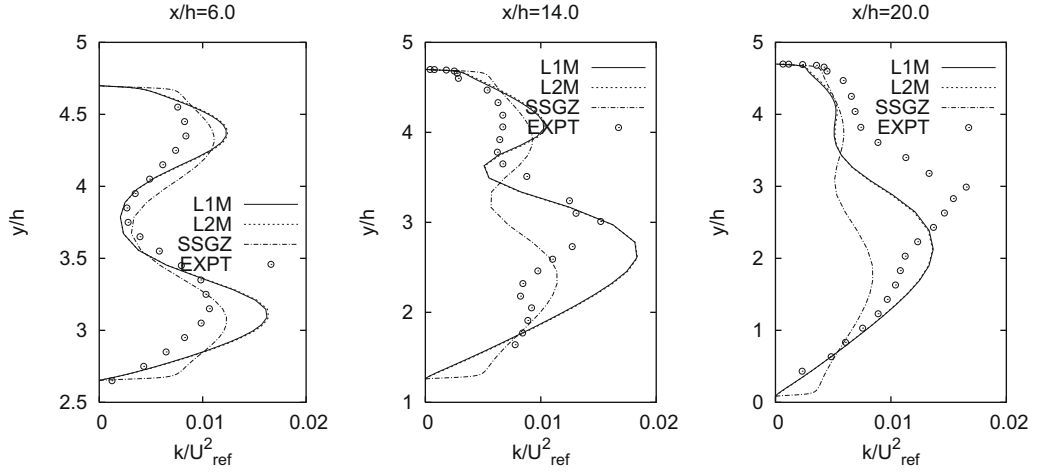

Fig. 16. Kinetic energy profiles at selected locations for diffuser flow.

velocity profiles is distinguishable. Unlike the SSGZ model, the present model predicts some anisotropy of turbulence due to the variation of C_μ in the eddy viscosity formulation, and hence yields results in better agreement with the data. However, compared with the experiment all models tend to gradually underpredict the peak for u-profile toward the outlet of the diffuser. Comparisons are extended to the distributions of Reynolds shear stress and the corresponding turbulent kinetic energy at different x/h locations, as displayed in Figs. 15 and 16. Since the $\overline{ww}$ component is not measured in the experiment, the usual approximation $k \approx 3/4(\overline{uu} + \overline{vv})$ is employed. A closer inspection of the distribution indicates that the present model predictions are in a broad agreement with the experimental data. The SSGZ has noticeable discrepancies with the measured data farther downstream. In fact, the flow inside the diffuser is characterized by strongly anisotropic turbulence. The inaccurately predicted mean velocity and turbulence profiles may largely be attributed to the models used which, by their linear nature, are unable to appropriately respond to strong anisotropy.

4. Conclusions

The new turbulence model is susceptible to the near-wall and low-Reynolds number effects issuing from the physical requirements. The elliptic relaxation function having different characteristic length scales replicates analogous results, indicating that the Kolmogorov length scale plays the major role for wall blocking. The eddy viscosity formulation depends nonlinearly on both the mean strain rate and vorticity invariants, and ensures realizability. The anisotropic production in the dissipation equation is accounted for substantially by modifying the model coefficients $C_{(\epsilon 1,2)}$ and adding a secondary source term, leading to a reduced level of turbulence generation in nonequilibrium flow regions. Consequently, the model is capable of evaluating the flow cases with separation and reattachment. Contrasting the predicted results with measurements demonstrates that the present model is a significant improvement over the constant C_μ model. The proposed model is wall distance free, tensorially invariant, frame-indifferent and applicable to arbitrary topology in conjunction with structured/unstructured grids.

References

Abe, K., Kondoh, T., Nagano, Y., 1997. On Reynolds-stress expression and near-wall scaling parameters for predicting wall and homogeneous turbulent shear flows. Int. J. Heat Fluid Flow 18 (3), 266–282.

Ahn, J.W., Park, T.S., Sung, H.J., 1997. Application of a near-wall turbulence model to the flows over a step with inclined wall. Int. J. Heat Fluid Flow 18 (2), 209–217.

Armfield, 1991. Finite difference solutions of the Navier-Stokes equations on staggered and non-staggered grids. Comput. Fluids 20 (1), 1–17.

Avva, R.K., Kline, S.J., Ferziger, J.H., 1988. Computation of the Turbulent Flow over a Backward-facing Step using the Zonal Modeling Approach. TF-33, Stanford University.

Bradbury, J.S., 1965. The structure of a self-preserving turbulent plane jet. J. Fluid Mech. 23 (1), 31–64.

Buice, C., Eaton, J.K., 1997. Experimental Investigation of Flow through an Asymmetric Plane Diffuser. Dept. of Mechanical Engineering, Thermoscience Div., Rept. TSD-107, Stanford University, California, CA.

Cazalbou, J.B., Bradshaw, P., 1993. Turbulent transport in wall bounded flows, evaluation of model coefficients using direct numerical simulation. J. Phys. Fluids 5, 3233–3239.

Chen, W.L., Lien, F.S., Leschziner, M.A., 1998. Nonlinear eddy viscosity modelling of transitional boundary layers pertinent to turbomachine aerodynamics. Int. J. Heat Fluid Flow 19 (4), 297–306.

Driver, D.M., Seegmiller, H.L., 1985. Features of a reattaching turbulent shear layer in divergent channel flow. AIAA J. 23 (2), 163–171.

Durbin, P.A., 1991. Near-wall turbulence closure modeling without damping functions. Theoret. Comput. Fluid Dynamics 3 (1), 1–13.

Durbin, P.A., Speziale, C.G., 1991. Local anisotropy in strained at high Reynolds numbers. J. Fluids Eng. 113, 707–709.

Durbin, P.A., 1993. A Reynolds-stress model for near-wall turbulence. J. Fluid Mech. 249, 465–498.

Durbin, P.A., Mansour, N.N., Yang, Z., 1994. Eddy viscosity transport model for turbulent flow. J. Phys. Fluids 6 (2), 1007–1015.

Durbin, P.A., 1995. Separated flow computations with $k-\epsilon-v^2$ model. AIAA J. 33 (4), 659–664.

Fares, E., Schröder, W., 2000. A differential equation for approximate wall distance. Int. J. Numer. Meth. Fluids 39 (8), 743–762.

Gatski, T.B., Speziale, C.G., 1993. On the explicit algebraic stress models for complex turbulent flows. J. Fluid Mech. 254, 59–78.

Girimaji, S.S., 1996. Fully explicit and self-consistent algebraic Reynolds stress model. Theoret. Comput. Fluid Dynamics 8 (6), 387–402.

Heskestad, G., 1965. Hot-wire measurements in a plane turbulent jet. J. Appl. Mech. 32, 721–734.

Jameson, A., Yoon, S., 1986. Multigrid solution of the Euler equations using implicit schemes. AIAA J. 24 (11), 1737–1743.

Jongen, T., Gatski, T.B., 1998. A New approach to characterizing the equilibrium states of the Reynolds stress anisotropy in homogeneous turbulence. Theoret. Comput. Fluid Dynamics 11 (1), 31–47.

Kim, J., Moin, P., Moser, R., 1987. Turbulence statistics in fully developed channel flow at low Reynolds number. J. Fluid Mech. 177, 133–166.

Launder, B.E., Sharma, B.I., 1974. Application of the energy dissipation model of turbulence to the calculation of flow near a spinning disc. Lett. Heat Mass Transfer 1, 131–138.

Lee, M.J., Kim, J., Moin, P., 1990. Structure of turbulence at high shear rate. J. Fluid Mech. 216, 561–583.

Lombard, C., Bardina, J., Venkatapathy, E., Oliger, J., 1983. Multi-dimensional formulation of CSCM - an upwind flux difference eigenvector split method for the compressible Navier-Stokes equations. In: 6th AIAA Computational Fluid Dynamics Conference, AIAA Paper 83-1895-CP, pp. 649–664.

Lumley, J.L., 1978. Computational modeling of turbulent flows. Adv. Appl. Mech. 18, 124–176.

Manceau, R., Wang, M., Laurence, D., 2001. Inhomogeneity and anisotropy effects on the redistribution term in Reynolds-averaged Navier-Stokes modelling. J. Fluid Mech. 438, 307–338.

Mansour, N.N., Kim, J., Moin, P., 1988. Reynolds-stress and dissipation-rate budgets in a turbulent channel flow. J. Fluid Mech. 194, 15–44.

Park, T.S., Sung, H.J., 1997. A new low-Reynolds number $k-\epsilon-f_\mu$ model for predictions involving multiple surface. Fluid Dynamics Res. 20, 97–113.

Patel, VC., Rodi, W., Scheuerer, G., 1985. Turbulence models for near-wall and low Reynolds number flow: a review. AIAA J. 23 (9), 1308–1319.

Pope, S.B., 1975. A more general effective viscosity hypothesis. J. Fluid Mech. 72, 331–340.

Rahman, M.M., Miettinen, A., Siikonen, T., 1996. Modified SIMPLE formulation on a collocated grid with an assessment of the simplified QUICK scheme. Numer. Heat Transfer B 30, 291–314.

Rahman, M.M., Rautaheimo, P., Siikonen, T., 1997. Numerical study of turbulent heat transfer from a confined impinging jet using a pseudo-compressibility method. In: Hanjalic, K., Peeters, T.W.J. (Eds.), Second International Symposium on Turbulence, Heat and Mass transfer, Delft University Press, Delft, The Netherlands, pp. 511–520.

Rahman, M.M., Siikonen, T., 2000. Improved low-Reynolds-number $k-\bar{\epsilon}$ model. AIAA J. 38 (7), 1298–1300.

Rahman, M.M., Siikonen, T., 2001. Modifications for an explicit algebraic stress model. Int. J. Numer. Meth. Fluids 35 (2), 221–245.

Rahman, M.M., Siikonen, T., 2001. An artificial compressibility method for incompressible flows. Numer. Heat Transfer B 40, 391–409.

Rahman, M.M., Siikonen, T., 2003. Near-wall turbulence modelling with enhanced dissipation. Int. J. Numer. Meth. Fluids 42 (9), 979–997.

Roach, P.E., Brierly, D.H., 1992. Test case T3A T3B Numerical Simulation of Unsteady and Transition to Turbulence. Cambridge University Press, Cambridge, London. p. 319.

Rodi, W., 1975. A new method for analyzing how-wire signals in highly turbulent flows and its evaluation on round jets. Disa Inform. 17, 9–18.

Roe, P.L., 1981. Approximate Riemann solvers parameter vectors and difference schemes. J. Comput. Phys. 43 (2), 357–372.

Rogers, M.M., Moin, P., 1987. The structure of the vorticity field in homogeneous turbulent flows. J. Fluid Mech. 176, 33–66.

Rung, T., Thiele, F., Fu, S., 1999. On the realizability on nonlinear Stress-strain relationships for Reynolds stress closures. Flow Turbulence Combust. 60 (4), 333–359.

Savill, A.M., 1993. Some recent progress in the turbulence modeling of by-pass transition. In: Speziale, C.G., Launder, B.E. (Eds.), Near-Wall Turbulent Flows, RMC So, Elsevier, pp. 829–848.

Shih, T.H., Zhu, J., Lumley, J.L., 1995. A new Reynolds stress algebraic equation model. Comput. Meth. Appl. Mech. Eng. 125 (1–4), 287–302.

So, R.M.C., Sarkar, A., Gerodimos, G., Zhang, J., 1997. A dissipation date equation for low-Reynolds number and near-wall turbulence. Theor. Comput. Fluid Dynamics 9 (1), 47–63.

Tavoularis, S., Corrsin, A., 1981. Experiments in nearly homogeneous turbulent shear flow with a uniform mean temperature gradient. Part I. J. Fluid Mech. 104, 311–347.

Tucker, P.G., 1998. Assessment of geometrical multilevel convergence robustness and a wall distance method for flows with multiple internal boundaries. Appl. Math. Model. 22 (4–5), 293–311.

Tucker, P.G., 2000. Prediction of turbulent oscillatory flows in complex systems. Int. J. Numer. Meth. Fluids 33 (6), 869–895.

Tucker, P.G., 2003. Differential equation based wall distance computation for DES and RANS. J. Comput. Phys. 190 (1), 229–248.
Tucker, P.G., Rumsey, C.K., Salart, P.R., Bartels, N., Biedron, R.T., 2005. Computations of wall distances based on differential equations. AIAA J. 43 (3), 539–549.
Wygnanski, I., Fiedler, H.E., 1969. Some measurements in self-preserving jet. J. Fluid Mech. 38 (3), 577–612.
Yap, C.R., 1987. Turbulent Heat and Momentum Transfer in Recirculating and Impinging Flows. Ph.D. Thesis, Faculty of Technology, University of Manchester.
Yoon, B., Chung, M., 1995. Computation of compression ram flow with a cross-diffusion modified k—ϵ model. AIAA J. 33, 1518–1520.
Yoshizawa, A., 1987. Statistical modeling of a transport equation for the kinetic energy dissipation rate. Phys. Fluids A 30 (3), 628–631.